Impact of UAV Trajectory on NOMA-Assisted Cellular-Connected UAV Networks

Nilupuli Senadhira*, Salman Durrani*, Xiangyun Zhou*, Nan Yang*, and Ming Ding†

*Research School of Electrical, Energy and Materials Engineering, The Australian National University, Canberra, Australia.
Emails: {nilupuli.senadhira, salman.durrani, xiangyun.zhou, nan.yang}@anu.edu.au.
†Data61, CSIRO, Australia. Email: ming.ding@data61.csiro.au

Abstract—The consideration of unmanned aerial vehicle (UAV) trajectory is of crucial importance in the performance evaluation of cellular-connected UAV networks. In this work, we consider a cellular-connected aerial user equipment (AUE) employed for surveillance and monitoring. The AUE moves along a given trajectory, while periodically transmitting to a terrestrial base station (BS) in the uplink, with a specific quality of service (QoS) requirement. To avoid the underutilization of spectrum resources, we enable simultaneous uplink transmissions of the AUE and a terrestrial user equipment (TUE) using power-domain uplink aerial-terrestrial non-orthogonal multiple access (NOMA). We take the trajectory of AUE into consideration and develop an analytical framework to compute the total rate coverage probability, i.e., the probability where both AUE and TUE are decoded, at a given transmission point in the trajectory. In addition, we numerically determine the minimum height of AUE to achieve a certain QoS constraint for different AUE target data rates and built-up areas. Our results show that, for a spiral trajectory, the minimum height increases as the AUE moves from cell center to the boundary, and as the severity of the environmental parameters increases.

I. INTRODUCTION

Due to recent advancements in unmanned aerial vehicle (UAV) technology in the industry sector, and latest standardization efforts by standardization bodies such as the 3rd Generation Partnership Project (3GPP), cellular-connected UAVs have attracted a lot of recent attention [1]. In this regard, seamless integration between the aerial user equipments (AUEs) and terrestrial user equipments (TUEs) in a traditional cellular network, is an important topic of research [1, 2].

Various approaches have been proposed in the literature to serve cellular-connected UAVs. These include, employing advanced cell sectorization and beamforming [3], massive multiple input multiple output (MIMO) [4] and co-ordinated multi-point (CoMP) transmission [5]. Studies in [3–5] generally assume dedicated resources allocated to AUEs, which may not be efficient due to the underutilization of spectrum resources. In this regard, non-orthogonal multiple access (NOMA) is a promising technique to address the resource scarcity issue [6]. While NOMA has been extensively considered in UAV-assisted wireless communications [7–10], where UAVs act as base stations or relays, only a few studies have investigated the impact of using NOMA in cellular-connected UAVs [11–13]. An uplink cooperative NOMA scheme to mitigate the

aerial-terrestrial interference between an AUE and multiple cellular BSs was proposed in [11]. The energy efficiency of a downlink NOMA scheme in a cellular network with both aerial and terrestrial users was investigated in [12]. A NOMA-based beamforming strategy was proposed in [13] to achieve high data rate transmission while avoiding inter-cell interference between the AUE and co-channel BSs in a cellular network. Note that, the coexistence of UAVs and TUEs was not addressed in [12], and mobility of UAVs was not considered in [11–13].

Mobility is an intrinsic characteristic of UAVs and the flight trajectory of UAVs must be properly accounted for in the design ad performance evaluation of UAV systems. Prior studies in the literature concerning UAV assisted wireless communication have assumed stationary UAVs [14] or stochastic trajectories [15–17], where the movement of UAVs is characterized by means of stochastic processes. Some studies have considered deterministic trajectories where an UAV is assumed to travel among know locations [18, 19]. For surveillance purposes, deterministic trajectory is more appropriate and adopted in this work. In addition, we are interested in whether the surveillance or monitoring data at each transmission point along the trajectory is successfully transmitted or not. To the best of our knowledge, this has not been investigated in the literature due to date for a cellular-connected UAV with NOMA.

Contributions: In this work, we consider a cellular-connected AUE employed for surveillance and monitoring a given area. The AUE transmits to the BS periodically in the uplink with a certain target data rate. Power-domain uplink aerial-terrestrial NOMA is used to facilitate simultaneous uplink transmission by the AUE and the existing TUE in the cellular network. The main contributions of this work are:

- Using stochastic geometry, we develop an analytical framework to evaluate the total rate coverage probability (i.e., the probability where both AUE and TUE are decoded) at a given transmission point along the AUE's trajectory. We also determine the minimum height of the AUE at each transmission point in the trajectory to achieve a certain quality of service (QoS) for various built-up environments.
- Our results show that, when the AUE follows a spiral trajectory, the total rate coverage probability decreases as the AUE moves from cell center to cell boundary, and when

the AUE's SINR threshold increases. Also, the minimum height increases as the AUE moves from cell center to the boundary. The QoS is satisfied along the entire trajectory for low to moderate AUE SINR thresholds for suburban, urban, and dense urban environments.

The results highlight the importance of suitably accounting for UAV's trajectory in cellular-connected UAV networks.

II. System model

We consider a single-cell wireless communication system with a terrestrial base station (BS), multiple terrestrial user equipment (TUEs) and an aerial user equipment (AUE), where the AUE is employed for surveillance purposes. We assume that each TUE is assigned an orthogonal time-frequency resource block in the uplink to transmit to the BS. Hence, there is no intra-cell interference among the TUEs in the cell. The AUE transmits periodically to the BS, and the target data rate requirement of this transmission varies depending on the nature of the surveillance. For efficient spectrum usage, we pair the AUE's transmission with a random TUE, referred to as the *active TUE*[1], and enable simultaneous uplink transmissions of AUE and the active TUE using NOMA. The single-cell is modeled as a disk region $\mathcal{S}$ with radius R. The BS is located at the center of the cell at a fixed height h_{BS}, i.e., with three-dimensional (3D) cartesian coordinates $(0, 0, h_{BS})$. The active TUE is randomly located in $\mathcal{S}$ at coordinates $(x_T, y_T, 0)$, where $r_T = \sqrt{x_T^2 + y_T^2}$ is the horizontal distance between the BS the active TUE.

AUE Trajectory Model: We assume that the AUE flies along a trajectory $\mathcal{T}$, to cover $\mathcal{S}$, with a constant speed v_A at an altitude h_A above the ground[2]. This is illustrated in Fig. 1. The AUE transmits N times, with time period T_A along the trajectory $\mathcal{T}$, i.e., $\mathcal{T} \triangleq \mathcal{T}[n]_{n=1}^N$ where n is the transmission point index. We define N as $N = \left\lfloor \frac{s(\mathcal{T}[N])}{v_A T_A} \right\rfloor$, where $s(\mathcal{T}[N])$ is the total path length of $\mathcal{T}$ and $\lfloor \cdot \rfloor$ is the floor function. $\mathcal{T}[n] = (x_{A,n}, y_{A,n}, h_A)$ denotes the cartesian coordinates of the location of the AUE at the $n-$th transmission point, where $r_{A,n} = \sqrt{x_{A,n}^2 + y_{A,n}^2}$ is the horizontal distance between the projection of the AUE on the ground and the BS.

Channel Model: The terrestrial channel is modeled as a combination of a large-scale path-loss attenuation with path-loss exponent α_T, and small-scale Rayleigh fading component, with fading power gain H_T. Due to the path-loss, the TUE's transmit signal power decays at the rate $d_T^{-\alpha_T}$, where $d_T = \sqrt{r_T^2 + h_{BS}^2}$ is the Euclidean distance between the TUE and the BS.

The air-to-cellular (A2C) channel is modeled as a combination of a probabilistic distance and height dependent large-

[1]Since we focus on the AUE pairing with a random TUE, an assumption on the number of TUEs and their mobility is not required. Also, we ignore inter-cell interference issues in this work. For a discussion on these issues, please refer to [24].

[2]Note that the AUE is capable of varying its height along the course of the trajectory. In Section V, we consider both the cases of AUE flying at a constant height and the case of AUE varying its height at each transmission point to achieve a certain quality of service.

scale path-loss and small-scale Nakagami-m fading, with fading power gain H_A. The path-loss for the line-of-sight (LoS) and non-line-of-sight (NLoS) transmission links are modeled separately. We use the probabilistic LoS model suggested in International Telecommunication Union (ITU) recommendation report [20] to determine the occurrence probabilities of LoS ($\mathbb{P}_{LoS}$) and NLoS ($1 - \mathbb{P}_{LoS}$) transmission links. The corresponding path-loss function is given by

$$\zeta_A = \begin{cases} \eta_L d_A^{-\alpha_L}, & \text{if LoS} \\ \eta_N d_A^{-\alpha_N}, & \text{if NLoS,} \end{cases} \quad (1)$$

where $d_A = \sqrt{r_A^2 + (h_A - h_{BS})^2}$ is the Euclidean distance between the BS and the AUE, η_ν, α_ν, $\nu \in \{L, N\}$ are the additional attenuation factors and path-loss exponents for LoS and NLoS channels. The fading parameters for the LoS and NLoS channels are denoted by m_L and m_N, respectively.

Received Signal: We assume that the TUE and AUE employ single omnidirectional antennas. Moreover, the BS beamforms toward the AUE and the active TUE simultaneously with associated antenna gains G_A and G_T, respectively, by employing a dual antenna array. Note that we consider ideal antenna modeling in this work.

The AUE transmits with fixed transmit power P_A, whereas active TUE uses the channel inversion power control. We assume that the BS has a receiver sensitivity of ρ_{min}. Therefore, the active TUE adjusts its transmit power such that the average signal power received at the BS is equal to the cutoff threshold ρ_T, where $\rho_T > \rho_{min}$. Hence, $P_T = \rho_T d_T^{\alpha_T}$.

Based on the aforementioned system model, the received signal at the BS due to an AUE located at coordinates $(x_{A,n}, y_{A,n}, h_A)$ and an active TUE located at coordinates $(x_T, y_T, 0)$ is

$$\Psi_{BS} = \sqrt{P_T d_T^{-\alpha_T} H_T G_T} \Psi_T + \sqrt{P_A \zeta_A H_A G_A} \Psi_A + \mathfrak{n}, \quad (2)$$

where $\mathfrak{n}$ is the additive white Gaussian noise with variance σ^2, and Ψ_ϱ, $\varrho \in \{T, A\}$ denotes the signal transmitted by active TUE and AUE, respectively.

III. Proposed NOMA Scheme

In order to enable simultaneous uplink transmissions of the AUE and the active TUE, we employ power-domain aerial-terrestrial uplink NOMA with successive interference cancellation (SIC) at the BS. We assume that perfect channel state information is available at the BS. We rely on the diversity of the small-scale fading of the active TUE and the AUE, and the high probability of LoS of the A2C link to distinguish between the received powers corresponding to the active TUE and the AUE. Also, we assume that the received signal power corresponding to the AUE is stronger than that of the active TUE, due to the favorable aerial LoS environment. Thus, we consider an adaptive decoding order where the AUE is decoded first at the BS. However, due to the dynamic nature of the aerial and terrestrial user, there could be occasions where the received power corresponding to the active TUE is greater than that of AUE (i.e., when the AUE in closer proximity to the cell edge is paired with a TUE that is located
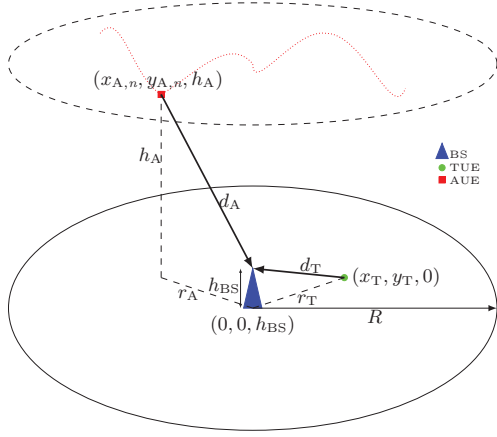
Fig. 1: Illustration of the 3D system model. AUE's arbitrary trajectory is illustrated by a red dotted line.

Fig. 2: Tree diagram of decoding events for proposed NOMA scheme.

close to the BS, the received signal power corresponding to the active TUE could be higher than that of the AUE). This is accounted for in our proposed NOMA scheme by adding an extra decoding step.

The tree diagram of the decoding events in the proposed NOMA scheme is illustrated in Fig. 2. It is explained as follows. The received signal at the BS is comprised of the superimposed Ψ_A and Ψ_T signals, where Ψ_A and Ψ_T denote the signals transmitted by the AUE and TUE, respectively. With SIC at the BS, Ψ_A is decoded first by treating Ψ_T as interference. If Ψ_A is decoded successfully, Ψ_T is decoded using SIC. Otherwise, BS tries to decode Ψ_T while treating Ψ_A as interference. In this work, we assume that, if Ψ_A is not decoded successfully, then error propagation occurs, i.e., BS treats the AUE's signal as interference when decoding Ψ_T. If Ψ_A is is decoded successfully, the error propagation factor is 0, i.e,. AUE's signal is reconstructed and subtracted from the superimposed signal [21]. If Ψ_T is decoded successfully at this stage, BS tries to decode the previously unsuccessful Ψ_A using SIC.

Each branch of the probability tree in Fig. 2 corresponds to a joint decoding event where either/ both/ none of the signals are decoded. Events corresponding to each branch are defined as follows:

- E_1 : Event that Ψ_A (i.e., AUE) is decoded in the first step and Ψ_T (i.e., TUE) is decoded in the second step.
- E_2 : Event that Ψ_A is decoded in the first step and Ψ_T is not decoded in the second step.
- E_3 : Event that Ψ_A is not decoded in the first step, Ψ_T is decoded in the second step, and Ψ_A is decoded in the third step.
- E_4 : Event that Ψ_A is not decoded in the first step, Ψ_T is decoded in the second step, and Ψ_A is not decoded in the third step.
- E_5 : Event that Ψ_A is not decoded in the first step and Ψ_T is not decoded in the second step.

Remark 1: Due to the extra decoding step (corresponding to events E_3 and E_4), the tree diagram in this work is different from the tree diagrams in prior works in terrestrial NOMA
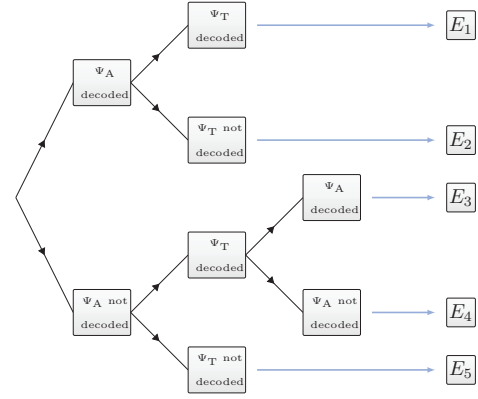
[22, 23]. In addition, we take the dependency of individual decoding steps into account rather than making the assumption that the decoding steps are independent as in [23].

IV. ANALYTICAL FRAMEWORK

In this section, we analyze the system performance using the total rate coverage probability as the performance metric [23].

Definition 1: The total rate coverage probability P_{Tot} is the probability that the achievable data rates of both the AUE and the active TUE exceed their corresponding target data rates. The rate coverage probability of a UE is defined as $\mathbb{P}(B \log_2(1 + \text{SINR}_\varrho) \geq \pi_\varrho)$, where $\varrho \in \{\text{T}, \text{A}\}$ denotes TUE and AUE, and B, SINR_ϱ and π_ϱ correspond to the bandwidth, signal-to-interference-plus-noise ratio and target data rate of the user, respectively.

For analytical simplicity, the rate coverage probability of a user can be re-formulated as $\mathbb{P}[\text{SINR}_\varrho \geq \theta_\varrho]$, which is the complementary cumulative distribution function (CCDF) of SINR, where $\theta_\varrho = 2^{\frac{\pi_\varrho}{B} - 1}$ is the target SINR threshold of the user.

We can evaluate the total rate coverage probability at each trajectory point of AUE, by evaluating the probability of the events where both AUE and TUE are successfully decoded, which correspond to events E_1 and E_3 of the proposed NOMA scheme[3]. Thus, the total rate coverage probability P_{Tot} can be calculated as

$$P_{\text{Tot}} = P_1 + P_3, \qquad (4)$$

where $P_i = \mathbb{P}(E_i)$, and $i = 1, 3$.

Next we present three Lemmas, which help to derive P_{Tot}.

Lemma 1: The probability density function (PDF) of the 3D propagation distance d_T between BS and TUE is

$$f_{d_T}(z) = \frac{2z}{R^2} , \; h_{\text{BS}} \leq z \leq \sqrt{R^2 + h_{\text{BS}}^2}. \qquad (5)$$

Proof: Proof is similar to that of Lemma 2 in [25]. ∎

Lemma 2: The cumulative distribution function (CDF) and PDF of the received power ψ_T corresponding to the active TUE are

---

[3]Note that the joint decoding events E_2 and E_4 contribute to the decoding of AUE and TUE alone. These decoding events were discussed in [24].

$$P_3 = \begin{cases} \exp\left(\frac{-\theta_\mathrm{T}\sigma^2}{\mu}\right)\left[\frac{\mathbb{P}_\mathrm{LoS}}{\Gamma(m_\mathrm{L})}\beta_\mathrm{L}^{m_\mathrm{L}}\left(\beta_\mathrm{L}+\frac{\theta_\mathrm{T}}{\mu}\right)^{-m_\mathrm{L}}\Gamma\left(m_\mathrm{L},\theta_\mathrm{A}\left(\beta_\mathrm{L}+\frac{\theta_\mathrm{T}}{\mu}\right)\sigma^2\right)\right. \\ \left.+\frac{1-\mathbb{P}_\mathrm{LoS}}{\Gamma(m_\mathrm{N})}\beta_\mathrm{N}^{m_\mathrm{N}}\left(\beta_\mathrm{N}+\frac{\theta_\mathrm{T}}{\mu}\right)^{-m_\mathrm{N}}\Gamma\left(m_\mathrm{N},\theta_\mathrm{A}\left(\beta_\mathrm{N}+\frac{\theta_\mathrm{T}}{\mu}\right)\sigma^2\right)\right], & \text{if } \theta_\mathrm{A}\theta_\mathrm{T}\geq 1 \\ \frac{\mathbb{P}_\mathrm{LoS}}{\Gamma(m_\mathrm{L})}\exp\left(\frac{\sigma^2}{\mu}\right)\beta_\mathrm{L}^{m_\mathrm{L}}\left(\beta_\mathrm{L}+\frac{1}{\theta_\mathrm{A}\mu}\right)^{-m_\mathrm{L}}\Gamma\left(m_\mathrm{L},\left(\beta_\mathrm{L}\theta_\mathrm{A}+\frac{1}{\mu}\right)\sigma^2\right) \\ +\frac{1-\mathbb{P}_\mathrm{LoS}}{\Gamma(m_\mathrm{N})}\exp\left(\frac{\sigma^2}{\mu}\right)\beta_\mathrm{N}^{m_\mathrm{N}}\left(\beta_\mathrm{N}+\frac{1}{\theta_\mathrm{T}\mu}\right)^{-m_\mathrm{N}}\Gamma\left(m_\mathrm{N},\left(\beta_\mathrm{N}\theta_\mathrm{A}+\frac{1}{\mu}\right)\sigma^2\right)-\frac{1}{2}\frac{\theta_\mathrm{A}\theta_\mathrm{T}^2\sigma^4(1+\theta_\mathrm{A})^2}{(1-\theta_\mathrm{A}\theta_\mathrm{T})}, & \text{if } 0\leq\theta_\mathrm{A}\theta_\mathrm{T}<1. \end{cases} \tag{3}$$

(a) $\theta_\mathrm{A}\theta_\mathrm{T}>1$ (b) $\theta_\mathrm{A}\theta_\mathrm{T}=1$ (c) $\theta_\mathrm{A}\theta_\mathrm{T}<1$
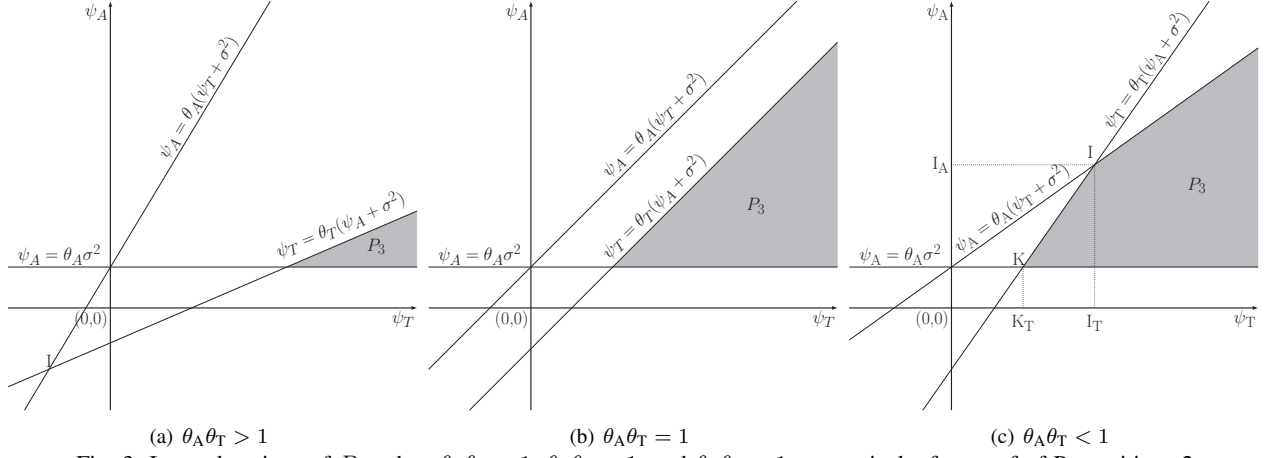
Fig. 3: Integral regions of P_3, when $\theta_\mathrm{A}\theta_\mathrm{T}>1$, $\theta_\mathrm{A}\theta_\mathrm{T}=1$, and $\theta_\mathrm{A}\theta_\mathrm{T}<1$, respectively, for proof of Propositions 2.

$$F_{\psi_\mathrm{T}}(x) = 1 - \exp\left(\frac{-x}{\rho_\mathrm{T}G_\mathrm{T}}\right), \tag{6}$$

and

$$f_{\psi_\mathrm{T}}(x) = \frac{1}{\rho_\mathrm{T}G_\mathrm{T}}\exp\left(\frac{-x}{\rho_\mathrm{T}G_\mathrm{T}}\right), \tag{7}$$

respectively, where $\psi_\mathrm{T} = P_\mathrm{T}d_\mathrm{T}^{-\alpha_\mathrm{T}}H_\mathrm{T}G_\mathrm{T}$.

Proof: See Appendix A. ∎

Lemma 3: The CDF and PDF of the received power ψ_A corresponding to the AUE are

$$F_{\psi_\mathrm{A}}(x) = 1 - \mathbb{P}_\mathrm{LoS}\sum_{i=0}^{m_\mathrm{L}-1}\frac{(\beta_\mathrm{L}x)^i}{i!}\exp(-\beta_\mathrm{L}x)$$
$$- (1-\mathbb{P}_\mathrm{LoS})\sum_{j=0}^{m_\mathrm{N}-1}\frac{(\beta_\mathrm{N}x)^j}{j!}\exp(-\beta_\mathrm{N}x), \tag{8}$$

and

$$f_{\psi_\mathrm{A}}(x) = \mathbb{P}_\mathrm{LoS}\frac{\exp(-x\beta_\mathrm{L})\beta_\mathrm{L}^{m_\mathrm{L}}x^{m_\mathrm{L}-1}}{\Gamma(m_\mathrm{L})}$$
$$+ (1-\mathbb{P}_\mathrm{LoS})\frac{\exp(-x\beta_\mathrm{N})\beta_\mathrm{N}^{m_\mathrm{N}}x^{m_\mathrm{N}-1}}{\Gamma(m_\mathrm{N})}, \tag{9}$$

where $\psi_\mathrm{A} = P_\mathrm{A}\zeta_\mathrm{A}H_\mathrm{A}G_\mathrm{A}$, $\beta_\mathrm{L} = \frac{m_\mathrm{L}}{P_\mathrm{A}\eta_\mathrm{L}d_\mathrm{A}^{-\alpha_\mathrm{L}}G_\mathrm{A}}$ and $\beta_\mathrm{N} = \frac{m_\mathrm{N}}{P_\mathrm{A}\eta_\mathrm{N}d_\mathrm{A}^{-\alpha_\mathrm{N}}G_\mathrm{A}}$.

Proof: See Appendix B. ∎

Next, we present the rate coverage probabilities of the joint decoding events E_1 and E_3, in order to evaluate P_Tot.

Proposition 1: The rate coverage probability P_1 of the joint decoding event E_1, where the AUE is decoded in the first step and TUE is decoded in the second step is

$$P_1 = \frac{1}{\mu}\exp\left(\frac{\sigma^2}{\mu}\right)\left[\mathbb{P}_\mathrm{LoS}\sum_{i=0}^{m_\mathrm{L}-1}\frac{(\beta_\mathrm{L}\theta_\mathrm{A})^i}{i!}\left(\beta_\mathrm{L}\theta_\mathrm{A}+\frac{1}{\mu}\right)^{-i-1}\right.$$

$$\times\Gamma\left(1+i,(1+\theta_\mathrm{T})\left(\beta_\mathrm{L}\theta_\mathrm{A}+\frac{1}{\mu}\right)\sigma^2\right)$$
$$+ (1-\mathbb{P}_\mathrm{LoS})\sum_{j=0}^{m_\mathrm{N}-1}\frac{(\beta_\mathrm{N}\theta_\mathrm{A})^j}{i!}\left(\beta_\mathrm{N}\theta_\mathrm{A}+\frac{1}{\mu}\right)^{-j-1}$$
$$\left.\times\Gamma\left(1+j,(1+\theta_\mathrm{T})\left(\beta_\mathrm{N}\theta_\mathrm{A}+\frac{1}{\mu}\right)\sigma^2\right)\right], \tag{10}$$

where $\mu = \rho_\mathrm{T}G_\mathrm{T}$.

Proof: The proof relies on stochastic geometry and is presented in Appendix C. ∎

Proposition 2: The rate coverage probability P_3 of the joint decoding event E_3, where the AUE is not decoded in the first step, TUE is decoded in the second step, and AUE is decoded in the third step is given as (3) at the top of this page.

Proof: The rate coverage probability P_3 is

$$P_3 = \mathbb{P}_{\psi_\mathrm{A},\psi_\mathrm{T}}\left(\frac{\psi_\mathrm{A}}{\sigma^2}\geq\theta_\mathrm{A},\frac{\psi_\mathrm{T}}{\psi_\mathrm{A}+\sigma^2}\geq\theta_\mathrm{T},\frac{\psi_\mathrm{A}}{\psi_\mathrm{T}+\sigma^2}<\theta_\mathrm{A}\right). \tag{11}$$

The inequalities in (11) are plotted in Fig. 3. P_3 is derived by calculating the area covered by all three curves. The point of intersection of $\psi_\mathrm{A} = \theta_\mathrm{A}(\psi_\mathrm{T}+\sigma^2)$ and $\psi_\mathrm{T} = \theta_\mathrm{T}(\psi_\mathrm{A}+\sigma^2)$ is given by $I = \left(\frac{\theta_\mathrm{T}\sigma^2(1+\theta_\mathrm{A})}{1-\theta_\mathrm{A}\theta_\mathrm{T}},\frac{\theta_\mathrm{A}\sigma^2(1+\theta_\mathrm{T})}{1-\theta_\mathrm{A}\theta_\mathrm{T}}\right)$. Depending on the value of $\theta_\mathrm{A}\theta_\mathrm{T}$, the point of intersection, I can be located in different quadrants or non-existent (in the case of $\theta_\mathrm{A}\theta_\mathrm{T}=1$). Thus, P_3 can have different values in these cases.

We first present the proof of P_3 when $\theta_\mathrm{A}\theta_\mathrm{T}\geq 1$.

$$P_3 = \mathbb{P}_{\psi_\mathrm{A},\psi_\mathrm{T}}\left(\psi_\mathrm{T}\geq\theta_\mathrm{T}(\psi_\mathrm{A}+\sigma^2),\psi_\mathrm{A}\geq\theta_\mathrm{A}\sigma^2\right) \tag{12a}$$
$$= \mathbb{E}_{\psi_\mathrm{A}}\left[\mathbb{P}_{\psi_\mathrm{T}}\left(\psi_\mathrm{T}\geq\theta_\mathrm{T}(a+\sigma^2),a\geq\theta_\mathrm{A}\sigma^2\right)\right]$$

TABLE I: Parameter values for results.

Symbol	Value	Symbol	Value
R	500 m	T_A	30 s
h_{BS}	30 m	P_A	0.1 W
σ^2	-100 dBm	G_A	1
ρ_T	-75 dBm	α_L	2.2
G_T	1	α_N	3.5
α_T	3.5	η_L	0 dB
v_A	15 m/s	η_N	13 dB
h_A	25 m, 120 m	m_L	5
m	3	m_N	1

$$= \int_{\theta_A \sigma^2}^{\infty} \mathbb{P}_{\psi_T}\left(\psi_T \geq \theta_T(a + \sigma^2)\right) f_{\psi_A}(a) da \tag{12b}$$

$$= \int_{\theta_A \sigma^2}^{\infty} \mathbb{P}_{H_T, d_T}\left(H_T \geq \frac{\psi_T(a + \sigma^2)}{P_T d_T^{-\alpha_T} G_T}\right) f_{\psi_A}(a) da$$

$$= \int_{\theta_A \sigma^2}^{\infty} \mathbb{E}_{d_T}\left[\exp\left(-\frac{\theta_T(a + \sigma^2)}{P_T d_T^{-\alpha_T} G_T}\right)\right] f_{\psi_A}(a) da \tag{12c}$$

$$= \int_{\theta_A \sigma^2}^{\infty}\left[\int_{h_{BS}}^{\sqrt{h_{BS}^2 + R^2}} \exp\left(-\frac{\theta_T(a + \sigma^2)}{\rho_T z^{\alpha_T} z^{-\alpha_T} G_T}\right)\left(\frac{2z}{R^2}\right) dz\right]$$
$$\times f_{\psi_A}(a) da$$

$$= \int_{\theta_A \sigma^2}^{\infty} \exp\left(\frac{-\theta_T(a + \sigma^2)}{\rho_T G_T}\right)\left[\frac{\mathbb{P}_{LoS}\exp(-a\beta_L)\beta_L{}^{m_L} a^{m_L - 1}}{\Gamma(m_L)}\right.$$
$$\left. + (1 - \mathbb{P}_{LoS})\frac{\exp(-a\beta_N)\beta_N{}^{m_N} a^{m_N - 1}}{\Gamma(m_N)}\right] da, \tag{12d}$$

where (12a) is the simplified expression for the area of P_3 based on Fig. 3(a) and 3(b). (12c) comes from the fact that H_T follows an exponential distribution. Integration of (12d) with respect to a and substitution of $\mu = \rho_T G_T$ into (12d) yields (3) for the case $\theta_A \theta_T \geq 1$.

The proof of P_3 for the case $\theta_A \theta_T < 1$ is similar to that of $\theta_A \theta_T \geq 1$ and a detailed derivation is given in [24]. ∎

V. NUMERICAL RESULTS

In this section we characterize the performance of the proposed NOMA scheme by investigating the impact of AUE SINR threshold, AUE altitude, and built-up environment on total rate coverage probability P_{Tot}. The parameter values used for the results are presented in Table I [25, 26]. We assume a bandwidth of 10 MHz and consider AUE target SINR thresholds $\{0, 10, 20, 30, 40\}$ dB which correspond to AUE target rates $\{10, 34.6, 66.6, 99.7, 134.6\}$ Mbps. We consider a target rate of 10 Mbps (corresponding to a target SINR threshold of 0 dB) for the TUE, unless stated otherwise.

Our framework is valid for any given trajectory. For the purpose of generating results, we model AUE's trajectory using an Archimedes' spiral, as it is an appropriate trajectory for monitoring or surveillance in a disk region. The AUE starts its spiral trajectory $\mathcal{T}$ at the center of the cell at a height h_A. In this case, $\mathcal{T}$ can be defined by $r_A = \frac{R}{2\pi m}\phi_A$, where m and ϕ_A, correspond to the number of rounds and orientation of AUE in the azimuth plane, measured with respect to the + x-axis, respectively. It is noted that r_A is derived based on the
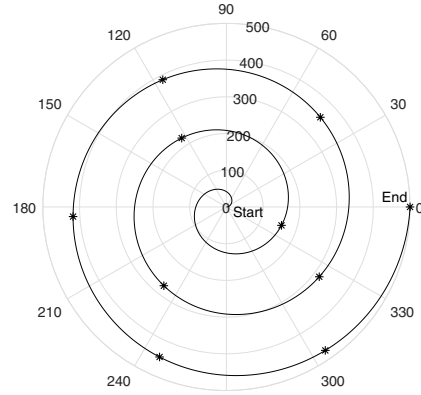

Fig. 4: Archimedes' spiral trajectory with $m = 3$ and $R = 500$ m. AUE's transmission points are denoted by asterisk ($v_A = 15$ m/s, $T_A = 30$ s).

assumption that the spiral starts at the center of the cell and reaches the cell edge at $\phi_{A\,Edge} = 2\pi m$ which is the maximum angle in the azimuth plane for a given number of rounds. Hence, the expressions for N and $r_{A,n}$ for the Archimedes' spiral are given as follows:

The number of transmission points along the AUE trajectory defined by the Archimedes' spiral is given by

$$N = \left\lfloor \frac{R\left(2\pi m\sqrt{1 + (2\pi m)^2} + \sinh^{-1}(2\pi m)\right)}{4\pi m v_A T_A}\right\rfloor. \tag{13}$$

The horizontal distance $r_{A,n}$ between the AUE and BS at the n-th transmission point is

$$r_{A,n} = R\sqrt{\frac{n}{N}}, \tag{14}$$

where $n = 1, \ldots, N$.

A. Model Validation

Fig. 5(a) and 5(b) show P_{Tot} at each trajectory point for different AUE SINR threshold values (θ_A) at $h_A = 25$ and 120 m, respectively. We can see that the simulation results match well with the analytical results. This verifies the accuracy of our analytical framework. For both heights, P_{Tot} decreases when θ_A is increased, and AUE moves away from the BS. The figure shows that the performance is better at $h_A = 120$ m (see Fig. 5(b)) compared to $h_A = 25$ m (see Fig. 5(a)). This is due to the fact that $\mathbb{P}_{LoS}$ is higher at $h_A = 120$ m compared to $h_A = 25$ m for the ITU probabilistic LoS model. The step-wise discrete behavior of P_{Tot} is due to the blockage caused by buildings in the built-up area in the ITU LoS model. This blockage behavior becomes smooth and continuous at very high altitude. Thus, this behavior is less prominent at $h_A = 120$ m.

B. Impact of AUE Altitude and Built-up Environments

In Fig. 5, we assumed that the AUE maintained a constant altitude along its entire trajectory. Now we allow the AUE to vary its height at each trajectory point in order to achieve
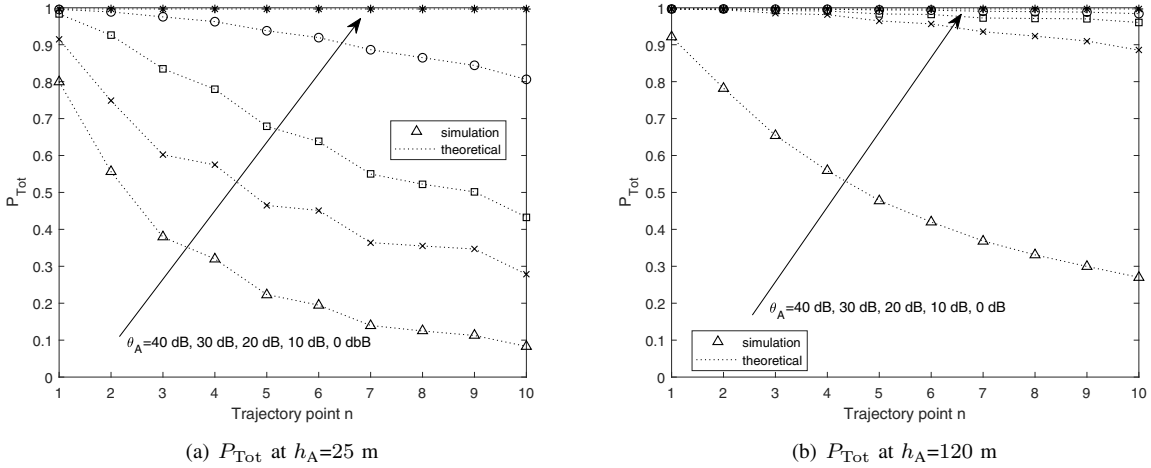
(a) P_{Tot} at $h_{\mathrm{A}}=25$ m

(b) P_{Tot} at $h_{\mathrm{A}}=120$ m

Fig. 5: P_{Tot} for (a) $h_{\mathrm{A}} = 25$ m and (b) $h_{\mathrm{A}} = 120$ m. The simulation values and the theoretical values are represented by markers and dotted lines, respectively.

a certain quality of service (QoS). QoS is defined as the probability where both AUE and TUE are decoded (equivalent to P_{Tot}). Current regulations in most countries do not permit AUEs to fly higher than a certain height. Therefore, we focus on the minimum altitude of AUE at each trajectory point, to achieve a QoS of 90% (corresponds to $P_{\mathrm{Tot}} = 0.9$) for different built-up environments.

Fig. 6 exhibits the minimum height of AUE to meet a QoS of 90% for different θ_{A} values in suburban, urban, and dense urban built-up environments. Note that the severity of the environmental parameters increases in the order of suburban, urban, and dense urban environments, respectively. That is to say, dense urban environment has a higher building to total area ratio, higher building density, and taller buildings compared to suburban environment. Fig. 6 shows that the AUE needs to ascend in order to achieve a QoS of 90% as the environment parameters become severe. For an instance, in suburban environment (see Fig. 6(a)), the QoS requirement is satisfied for all θ_{A} values along the entire trajectory at a lower height of 25 m, whereas for urban and dense urban environments (see Fig. 6(b) and 6(c), respectively), the AUE needs to ascend as the θ_{A} increases and the AUE moves from cell center to cell edge. While it is possible to achieve a QoS of 90% by increasing AUE's altitude for low to moderate θ_{A} values ($0 - 30$ dB), at 40 dB, the QoS cannot be satisfied even at a maximum altitude of 300 m.

VI. CONCLUSION

In this paper, we considered an AUE that moves along a given trajectory while periodically transmitting in uplink to the BS, concurrently with a TUE. We employed power domain uplink aerial-terrestrial NOMA to facilitate the simultaneous uplink transmissions of the AUE and the TUE. We derived analytical results for the total rate coverage probability which is the probability where both the AUE and the TUE are decoded, and it was validated by simulations. Our results showed that the total rate coverage probability decreases as the AUE moves from cell center to cell boundary, and when the AUE's SINR threshold increases. We also determined

the minimum height of AUE to achieve a QoS of 90% at each transmission point. The results showed that this height increases when the distance between the AUE and the BS increases, and as the severity of environmental parameters increases.

APPENDIX A
PROOF OF LEMMA 2

The CDF of ψ_{T} can be written as

$$F_{\psi_{\mathrm{T}}}(x) = \mathbb{P}_{d_{\mathrm{T}},H_{\mathrm{T}}} \left(P_{\mathrm{T}} d_{\mathrm{T}}^{-\alpha_{\mathrm{T}}} H_{\mathrm{T}} G_{\mathrm{T}} < x \right)$$

$$= \mathbb{E}_{d_{\mathrm{T}}} \left[1 - \exp\left(\frac{x}{P_{\mathrm{T}} d_{\mathrm{T}}^{-\alpha_{\mathrm{T}}} G_{\mathrm{T}}} \right) \right] \tag{15a}$$

$$= 1 - \int_{h_{\mathrm{BS}}}^{\sqrt{h_{\mathrm{BS}}^2 + R^2}} \exp\left(\frac{-x}{\rho_{\mathrm{T}} z^{\alpha_{\mathrm{T}}} z^{-\alpha_{\mathrm{T}}} G_{\mathrm{T}}} \right) \left(\frac{2z}{R^2} \right) dz, \tag{15b}$$

where (15a) comes from the fact that H_{T} follows an exponential distribution. (15b) is the expectation with respect to d_{T}, where $P_{\mathrm{T}} = \rho_{\mathrm{T}} z^{-\alpha_{\mathrm{T}}}$ and $f_{d_{\mathrm{T}}}(z) = \frac{2z}{R^2}$. Taking the derivative of $F_{\psi_{\mathrm{T}}}(x)$ with respect to x we obtain its PDF.

APPENDIX B
PROOF OF LEMMA 3

The CDF of ψ_{A} is expressed as $F_{\psi_{\mathrm{A}}}(x) = \mathbb{P}_{H_{\mathrm{A}},d_{\mathrm{A}}} \left(P_{\mathrm{A}} \zeta_{\mathrm{A}} H_{\mathrm{A}} G_{\mathrm{A}} < x \right) = \mathbb{E}_{d_{\mathrm{A}}} \left[\mathbb{P}\left(H_{\mathrm{A}} < \frac{x}{P_{\mathrm{A}} \zeta_{\mathrm{A}} G_{\mathrm{A}}} \right) \right]$. This can be simplified by substituting the CDF of H_{A}, where H_{A} follows a Gamma distribution with parameters m_{L} and m_{N} for LoS and NLoS A2C channel links, respectively. $f_{\psi_{\mathrm{A}}}(x)$ can be derived by taking the derivative of $F_{\psi_{\mathrm{A}}}(x)$ with respect to x.

APPENDIX C
PROOF OF PROPOSITION 1

The rate coverage probability P_1 can be expressed as

$$P_1 = \mathbb{P}_{\psi_{\mathrm{A}},\psi_{\mathrm{T}}} \left(\frac{\psi_{\mathrm{T}}}{\sigma^2} \geq \theta_{\mathrm{T}}, \frac{\psi_{\mathrm{A}}}{\psi_{\mathrm{T}} + \sigma^2} \geq \theta_{\mathrm{A}} \right)$$

$$= \mathbb{E}_{\psi_{\mathrm{T}}} \left[\mathbb{P}_{\psi_{\mathrm{A}}} \left(t \geq \theta_{\mathrm{T}} \sigma^2, \psi_{\mathrm{A}} \geq \theta_{\mathrm{A}}(t + \sigma^2) \right) \right] \tag{16a}$$

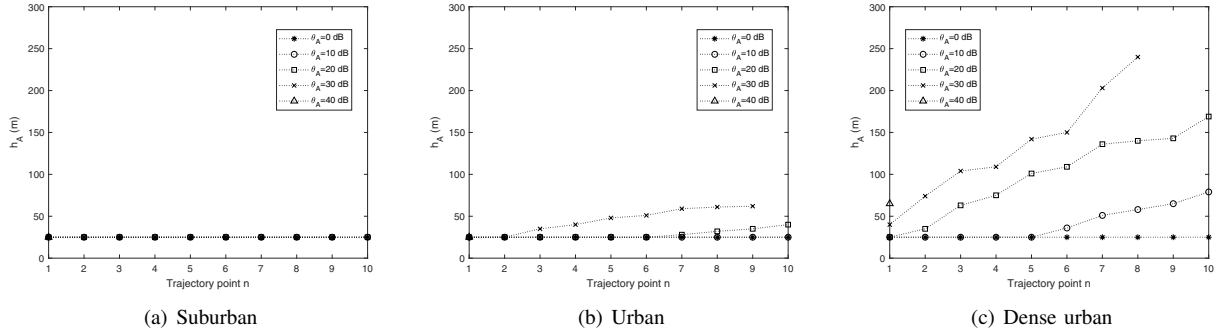(a) Suburban   (b) Urban   (c) Dense urban

Fig. 6: Minimum height of AUE to achieve a total rate coverage probability of 0.9 vs. the trajectory point for (a) suburban, (b) urban, and (c) dense urban environments. The environmental parameters, corresponding to different built-up areas with different building densities and heights in the ITU model, are given in Table 1 in [26].

$$= \int_{\theta_{\mathrm{T}}\sigma^2}^{\infty} \mathbb{P}\left(H_{\mathrm{A}} \geq \frac{\theta_{\mathrm{A}}(t+\sigma^2)}{P_{\mathrm{A}}\zeta_{\mathrm{A}}G_{\mathrm{A}}}\right) f_{\psi_{\mathrm{T}}}(t)dt \tag{16b}$$

$$= \int_{\theta_{\mathrm{T}}\sigma^2}^{\infty} \left(\mathbb{P}_{\mathrm{LoS}} \sum_{i=0}^{m_{\mathrm{L}}-1} \frac{(\beta_{\mathrm{L}}\theta_{\mathrm{A}})^i}{i!}(t+\sigma^2)^i \exp\left(-\beta_{\mathrm{L}}\theta_{\mathrm{A}}(t+\sigma^2)\right) \right.$$

$$\left. + (1-\mathbb{P}_{\mathrm{LoS}}) \sum_{j=0}^{m_{\mathrm{N}}-1} \frac{(\beta_{\mathrm{N}}\theta_{\mathrm{A}})^j}{i!}(t+\sigma^2)^j \exp\left(-\beta_{\mathrm{N}}\theta_{\mathrm{A}}(t+\sigma^2)\right)\right)$$

$$\times f_{\psi_{\mathrm{T}}}(t)dt, \tag{16c}$$

In (16a), we consider that t denotes a random variable with distribution $f_{\psi_{\mathrm{T}}}(t)$ and is a constant with respect to the random variable ψ_{A}.(16c) comes from the fact that the fading of AUE has a Gamma distribution. Finally, (10) can be derived by simplifying (16c) and substituting $\mu = \rho_{\mathrm{T}}G_{\mathrm{T}}$ into (16c).

REFERENCES

[1] Y. Zeng, Q. Wu, and R. Zhang, "Accessing From The Sky: A Tutorial on UAV Communications for 5G and Beyond," *arXiv:1903.05289*, Mar. 2019.

[2] Y. Zeng, J. Lyu, and R. Zhang, "Cellular-connected UAV: potential, challenges, and promising technologies," *IEEE Wirel. Commun.*, vol. 26, no. 1, pp. 120–127, Feb. 2019.

[3] X. Lin, V. Yajnanarayana, S. D. Muruganathan, S. Gao, H. Asplund, H. Maattanen, M. Bergstrom, S. Euler, and Y. . E. Wang, "The sky is not the limit: LTE for unmanned aerial vehicles," *IEEE Commun. Mag.*, vol. 56, no. 4, pp. 204–210, Apr. 2018.

[4] A. Garcia-Rodriguez, G. Geraci, D. Lopez-Perez, L. G. Giordano, M. Ding, and E. Bjornson, "The essential guide to realizing 5G-connected UAVs with massive MIMO," *IEEE Commun. Mag.*, pp. 2–8, Oct. 2019.

[5] R. Amer, W. Saad, H. ElSawy, M. Butt, and N. Marchetti, "Caching to the sky: Performance analysis of cache-assisted CoMP for cellular-connected UAVs," *arXiv:1811.11098*, Nov. 2018.

[6] L. Dai, B. Wang, Z. Ding, Z. Wang, S. Chen, and L. Hanzo, "A survey of non-orthogonal multiple access for 5G," *IEEE Commun. Surveys Tuts.*, vol. 20, no. 3, pp. 2294–2323, May 2018.

[7] Y. Liu, Z. Qin, Y. Cai, Y. Gao, G. Y. Li, and A. Nallanathan, "UAV communications based on non-orthogonal multiple access," *IEEE Wirel. Commun.*, vol. 26, no. 1, pp. 52–57, Feb. 2019.

[8] N. Rupasinghe, Y. Yapıcı, I. Güvenç, and Y. Kakishima, "Non-orthogonal multiple access for mmwave drone networks with limited feedback," *IEEE Trans. Commun.*, vol. 67, no. 1, pp. 762–777, Jan. 2019.

[9] R. Duan, J. Wang, C. Jiang, H. Yao, Y. Ren, and Y. Qian, "Resource allocation for Multi-UAV aided IoT NOMA uplink transmission systems," *IEEE Internet Things J.*, Aug. 2019.

[10] J. Sun, Z. Wang, and Q. Huang, "Cyclical NOMA based UAV-enabled wireless network," *IEEE Access*, vol. 7, pp. 4248–4259, Dec. 2019.

[11] W. Mei and R. Zhang, "Uplink cooperative NOMA for cellular-connected UAV," *IEEE J. Sel. Topics Signal Process.*, vol. 13, no. 3, pp. 644–656, Jun. 2019.

[12] A. Rahmati, Y. Yapici, N. Rupasinghe, I. Guvenc, H. Dai, and A. Bhuyan, "Energy efficiency of RSMA and NOMA in cellular-connected mmWave UAV networks," in *Proc. IEEE ICC Workshops*, May 2019.

[13] L. Liu, S. Zhang, and R. Zhang, "Exploiting NOMA for multi-beam UAV communication in cellular uplink," in *Proc. IEEE ICC*, May 2019, pp. 1–6.

[14] V. V. Chetlur and H. S. Dhillon, "Downlink coverage analysis for a finite 3-D wireless network of unmanned aerial vehicles," *IEEE Trans. Commun.*, vol. 65, no. 10, pp. 4543–4558, Oct. 2017.

[15] S. Enayati, H. Saeedi, H. Pishro-Nik, and H. Yanikomeroglu, "Moving aerial base station networks: A stochastic geometry analysis and design perspective," *IEEE Trans. Wireless Commun.*, vol. 18, no. 6, pp. 2977–2988, Jun. 2019.

[16] P. K. Sharma and D. I. Kim, "Coverage probability of 3-D mobile UAV networks," *IEEE Wireless Commun. Lett.*, vol. 8, no. 1, pp. 97–100, Feb. 2019.

[17] M. Banagar and H. S. Dhillon, "3GPP-inspired stochastic geometry-based mobility model for a drone cellular network," in *Proc. IEEE GLOBECOM*, Dec. 2019.

[18] M. M. U. Chowdhury, E. Bulut, and I. Guvenc, "Trajectory optimization in UAV-assisted cellular networks under mission duration constraint," in *Proc. IEEE RWS*, Jan. 2019, pp. 1–4.

[19] D. Yang, Q. Wu, Y. Zeng, and R. Zhang, "Energy tradeoff in ground-to-UAV communication via trajectory design," *IEEE Trans. Veh. Technol.*, vol. 67, no. 7, pp. 6721–6726, Jul. 2018.

[20] ITU, "Recommendation p.1410-5: Propagation data and prediction methods required for the design of terrestrial broadband radio access systems operating in a frequency range from 3 to 60 GHz," *Tech, Rep*, Feb. 2012.

[21] H. Sun, B. Xie, R. Q. Hu, and G. Wu, "Non-orthogonal multiple access with SIC error propagation in downlink wireless MIMO networks," in *Proc. VTC-Fall*, Sep. 2016.

[22] B. Xia, J. Wang, K. Xiao, Y. Gao, Y. Yao, and S. Ma, "Outage performance analysis for the advanced SIC receiver in wireless NOMA systems," *IEEE Trans. Veh. Technol.*, vol. 67, no. 7, pp. 6711–6715, Jul. 2018.

[23] H. Tabassum, E. Hossain, and J. Hossain, "Modeling and analysis of uplink non-orthogonal multiple access in large-scale cellular networks using Poisson cluster processes," *IEEE Trans. Commun.*, vol. 65, no. 8, pp. 3555–3570, Aug. 2017.

[24] N. Senadhira, S. Durrani, X. Zhou, N. Yang, and M. Ding, "Uplink NOMA for Cellular-Connected UAV: Impact of UAV Trajectories and Altitude," *arXiv*, Oct. 2019.

[25] X. Zhou, S. Durrani, J. Guo, and H. Yanikomeroglu, "Underlay drone cell for temporary events: Impact of drone height and aerial channel environments," *IEEE Internet Things J.*, vol. 6, no. 2, pp. 1704–1718, Apr. 2019.

[26] J. Holis and P. Pechac, "Elevation dependent shadowing model for mobile communications via high altitude platforms in built-up areas," *IEEE Trans. Antennas Propag*, vol. 56, no. 4, pp. 1078–1084, Apr. 2008.